PAPER

Interference structure of above-threshold ionization versus above-threshold detachment

New Journal of Physics
The open-access journal for physics

Interference structure of above-threshold ionization versus above-threshold detachment

Ph A Korneev[1], S V Popruzhenko[1], S P Goreslavski[1], W Becker[2], G G Paulus[3], B Fetić[4] and D B Milošević[2,4,5,6]

[1] National Research Nuclear University MEPhI, Kashirskoe Shosse 31, 115409 Moscow, Russia
[2] Max-Born-Institut, Max-Born-Strasse 2a, 12489 Berlin, Germany
[3] Institute of Optics and Quantum Electronics, Friedrich Schiller University, Max-Wien-Platz 1, 07743 Jena, Germany
[4] Faculty of Science, University of Sarajevo, Zmaja od Bosne 35, 71000 Sarajevo, Bosnia and Hercegovina
[5] Academy of Sciences and Arts of Bosnia and Hercegovina, Bistrik 7, 71000 Sarajevo, Bosnia and Hercegovina
E-mail: milo@bih.net.ba

New Journal of Physics **14** (2012) 055019 (16pp)
Received 5 March 2012
Published 21 May 2012
Online at http://www.njp.org/
doi:10.1088/1367-2630/14/5/055019

Abstract. Laser-induced electron detachment or ionization of atoms and negative ions is considered. In the context of the saddle-point evaluation of the strong-field approximation (SFA), the velocity maps of the direct electrons (those that do not undergo rescattering) exhibit a characteristic structure due to the constructive and destructive interference of electrons liberated from their parent atoms/ions within certain windows of time. This structure is defined by the above-threshold ionization rings at fixed electron energy and by two sets of curves in momentum space on which destructive interference occurs. The spectra obtained with the SFA are compared with those obtained by numerical solution of the time-dependent Schrödinger equation. For detachment, the agreement is excellent. For ionization, the effect of the Coulomb field is most pronounced for electrons emitted in a direction close to laser polarization, while for near-perpendicular emission the qualitative appearance of the spectrum is unaffected.

[6] Author to whom any correspondence should be addressed.

Contents

1. Introduction

Multiphoton ionization or detachment is the basic process that occurs if an atom or negative ion is exposed to an intense laser field. The resulting electron spectrum, represented in the form of an angle-resolved energy spectrum or as a velocity map, has been the challenging object of various approaches to the description of the laser–matter interaction, especially since the first observation of above-threshold ionization (ATI) [1]. The spectrum strongly depends on the wavelength and intensity of the driving laser field. Ever since the seminal work of Keldysh [2] and Perelomov *et al* [3], two limiting cases have been distinguished. For comparatively low intensity and/or high frequency, the electron reaches its final state by absorbing just the minimum number of laser photons possible (the so-called multi-photon limit). In this case, the resulting angular distribution is given by the superposition of a few eigenstates of angular momentum. In the opposite limit of high intensity and/or low frequency (the so-called tunneling limit), the electron can be envisioned to tunnel into the continuum through the effective-potential barrier generated by the laser–electron potential and the atomic or ionic binding potential. In this case, the final electron state is the superposition of a large number of angular-momentum states. These two cases should not be considered as different mechanisms (multi-photon versus tunneling) but rather as two different perspectives of the same physical process—ionization by an approximately monochromatic field. In this paper, we will be concerned with the high-intensity case. We also restrict ourselves to 'direct' electrons, which are defined as those that, after ionization, do not rescatter off the potential that bound them [4, 5].

As the longest-known multi-photon process in laser–atom physics, ATI has attracted much attention over the years, and a large number of data have been accumulated; for a more recent review, see [6]. The presentation of the data in the form of velocity maps has become standard [7–10], since these display many features of the data, especially for low energy and in the rescattering regime [11], more clearly than the usual angle-resolved energy spectra.

The theoretical complexity of the ionization process is due to the interplay of the binding potential and the laser field. Either field by itself provides a straightforward problem, analytically solvable in many cases, but the combined action of both fields does not allow such a solution. The strong-field approximation (SFA) [2, 3, 12–15] cuts through this complexity by, in effect, defining an instant of ionization such that before this time the electron is assumed only to feel the binding potential, while thereafter its motion is governed by the laser field alone.

The corresponding ionization amplitude is an integral over this time. For a given final (outside the field) momentum $\mathbf{p}$ of the electron, the integral can be evaluated by the method of steepest descent, which determines the corresponding ionization times $t_i(\mathbf{p})$. These times are the start times of electron orbits in the presence of the laser field—the so-called quantum orbits [16]. Arguably, the analysis of the data in terms of these quantum orbits provides the best way of intuitively understanding the quantum process of ionization [10, 17–19].

For direct electrons and a monochromatic laser field, which depends sinusoidally on time, there are exactly two such ionization times per laser period and therefore two quantum orbits for any given final momentum. Their contributions add coherently to the ionization amplitude or, more physically formulated, the corresponding wave packets interfere [20]. The resulting angle-resolved spectrum or velocity map is dominated by this interference pattern [19, 21]. The analytical calculation of this pattern on the basis of the SFA and the comparison with *ab initio* solutions obtained by solving the time-dependent Schrödinger equation (TDSE) are the theme of this paper. We expect major differences between the ionization of an atom and the detachment of a negative ion, owing to the absence of the long-range (Coulombic) binding potential in the latter case.

In this paper, we will not be concerned with the contribution of rescattering processes. For above-threshold detachment (ATD) and the relatively low energies which we are considering here, these are completely inessential. Of course, they dominate the spectrum for higher energies where the direct electrons do not contribute [22]. For ATI, the same statements essentially hold. However, for very low energies and parameters such that the so-called low-energy structure (LES) appears [23–25], the distinction between direct and rescattered electrons becomes questionable, owing to the behavior of the Coulomb scattering cross-section. There is also a rescattering contribution with very short travel time which is still unexplored (the so-called L orbits in high-order harmonic generation [26]).

This paper is organized as follows. In section 2, we recall the SFA in the saddle-point approximation and proceed to derive the geometrical curves on which the two relevant quantum orbits interfere destructively. We also obtain a formula that specifies the number of interference minima on a given ATI ring. In section 3, we present our results. We choose the negative F and H ions as illustrations for ATD and the H atom for ATI and compare in each case the SFA spectra with those obtained by numerical solution of the TDSE. The agreement is excellent for ATD, which establishes the SFA as a completely reliable calculational method in this case. This is not so in the presence of the long-range Coulomb potential where, however, some features predicted by the SFA do survive. We present the conclusions in section 4. We use atomic units so that $\hbar = 1$, $m = 1$, $|e| = 1$ and $4\pi\epsilon_0 = 1$ throughout the paper.

2. Matrix element in the strong-field approximation

The transition amplitude from the atomic or ionic ground state $|\psi_\ell(t)\rangle = |\psi_\ell\rangle \exp(\mathrm{i}I_p t)$, having the parity $(-1)^\ell$ and the ionization potential I_p, to the final continuum state $|\mathbf{p}\rangle$, both in the absence of the laser field, is [2, 3, 5, 12, 13]

$$M_{\mathbf{p}} = \int_{-\infty}^{\infty} \mathrm{d}t \, \langle \psi_{\mathbf{p}}^{(\mathrm{V})}(t)|V(\mathbf{r})|\psi_\ell(t)\rangle$$
$$= \int_{-\infty}^{\infty} \mathrm{d}t \, V(\mathbf{p}, t) \mathrm{e}^{\mathrm{i}S(\mathbf{p},t)}, \tag{1}$$

where

$$|\psi_{\mathbf{p}}^{(\mathrm{V})}(t)\rangle = |\mathbf{p}+\mathbf{A}(t)\rangle \mathrm{e}^{-\mathrm{i}\int^t \mathrm{d}\tau[\mathbf{p}+\mathbf{A}(\tau)]^2/2} \tag{2}$$

is the Volkov solution in length gauge with $\langle \mathbf{r}|\mathbf{p}\rangle = (2\pi)^{-3/2}\exp(\mathrm{i}\mathbf{p}\cdot\mathbf{r})$ a plane wave,

$$S(\mathbf{p},t) = \frac{1}{2}\int^t \mathrm{d}\tau[\mathbf{p}+\mathbf{A}(\tau)]^2 + I_\mathrm{p}t \tag{3}$$

is the action and

$$V(\mathbf{p},t) = (2\pi)^{-3/2}\int \mathrm{d}^3\mathbf{r}\,\mathrm{e}^{-\mathrm{i}[\mathbf{p}+\mathbf{A}(t)]\cdot\mathbf{r}} V(\mathbf{r})\psi_\ell(\mathbf{r}). \tag{4}$$

For sufficiently high intensity and low frequency, temporal integration in the matrix element (1) is conveniently carried out with the help of the method of steepest descent. This yields

$$M_\mathbf{p} = \sum_i a_i(\mathbf{p})\exp[\mathrm{i}S_i(\mathbf{p})] \tag{5}$$

with $S_i(\mathbf{p}) \equiv S(\mathbf{p},t_i)$, and $t_i \equiv t_i(\mathbf{p})$ being a solution to the saddle-point equation

$$\tfrac{1}{2}\left\{p_\perp^2 + [p_\parallel + A(t)]^2\right\} = -I_\mathrm{p}. \tag{6}$$

We assume a linearly polarized laser field with the vector potential $\mathbf{A}(t)$, and $p_\parallel$ and $p_\perp$ denote the components of the final momentum $\mathbf{p}$ parallel and perpendicular to $\mathbf{A}(t)$. The prefactor of the exponential in equation (5) is

$$a_i(\mathbf{p}) = \left\{\frac{2\pi}{\mathrm{i}[\mathbf{p}+\mathbf{A}(t_i)]\cdot\mathbf{E}(t_i)}\right\}^{1/2} V(\mathbf{p},t_i). \tag{7}$$

For the linearly polarized monochromatic field

$$A(t) = A_0\cos\omega t, \tag{8}$$

with the ponderomotive potential $U_\mathrm{p} = A_0^2/4$, there are two solution times t_1 and t_2 ($\mathrm{Re}\,t_2 > \mathrm{Re}\,t_1$, $\mathrm{Im}\,t_i > 0$) per cycle of the saddle-point equation (6), which satisfy

$$\mathrm{Re}\,\omega t_2 = 2\pi - \mathrm{Re}\,\omega t_1, \quad \mathrm{Im}\,\omega t_1 = \mathrm{Im}\,\omega t_2. \tag{9}$$

An example of such solutions is shown in figure 1.

The electron spectrum has the form of concentric rings in the momentum plane. These rings are centered at zero momentum and correspond to the characteristic ATI peaks. Each ring can be envisioned as due to the net absorption of a specific number N of photons from the laser field. The minimum number of absorbed photons necessary for ionization is $N_\mathrm{min} = [(I_\mathrm{p}+U_\mathrm{p})/\omega]+1$, where $[x]$ denotes the integer part of x. The electron energy on the $(N-N_\mathrm{min}+1)$th ring is

$$E = (p_\perp^2 + p_\parallel^2)/2 = N\omega - I_\mathrm{p} - U_\mathrm{p}. \tag{10}$$

For the two saddle-point times (9), the first factor of equation (7) is real and identical up to the small imaginary part of $\mathbf{E}(t_i)$, which we neglect. The second factors are equal for an even-parity ground state $|\psi_\ell\rangle$ and equal in magnitude but opposite in sign for an odd-parity ground state, i.e. $V(\mathbf{p},t_2) = (-1)^\ell V(\mathbf{p},t_1)$ (for $p_\parallel = 0$) [28].

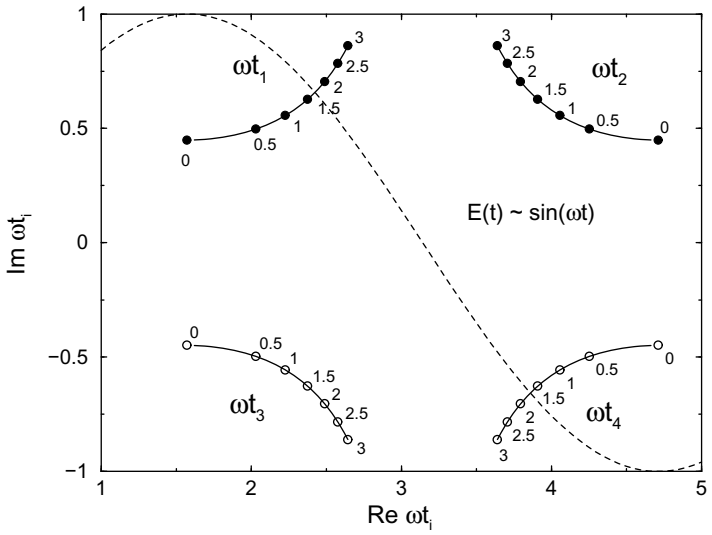

Figure 1. The saddle-point solutions t_i, $i = 1, \ldots, 4$, for the field (8) in the complex plane as functions of the drift energy $p_\parallel^2/2$ for $p_\perp = 0$ and $0 \leqslant p_\parallel^2/2 \leqslant 3U_\mathrm{p}$. The value of the Keldysh parameter is $\gamma = 0.464$. The physical solutions, which enter equation (1), are those in the upper half-plane. The electric field $E(t)$ is shown by the dashed line. From [27].

2.1. Destructive interference curves

If we assume that the complex weights (7) of the two quantum orbits are equal, then the interference of the two quantum orbits in the ionization amplitude will be destructive if

$$\mathrm{Re}\,\Delta S \equiv \mathrm{Re}\,[S_2(\mathbf{p}) - S_1(\mathbf{p})] = m\pi, \tag{11}$$

where m is odd for even ground-state parity and is even for odd parity. We have

$$\Delta S = \left[\frac{1}{2}(p_\parallel^2 + p_\perp^2) + I_\mathrm{p}\right](t_2 - t_1) + p_\parallel \int_{t_1}^{t_2} \mathrm{d}\tau\, \mathrm{A}(\tau) + \frac{1}{2}\int_{t_1}^{t_2} \mathrm{d}\tau\, \mathrm{A}(\tau)^2. \tag{12}$$

The condition (11) defines curves in the $(p_\perp, p_\parallel)$ space, which we will now investigate in more detail.

In order to stay on such a curve as we vary $p_\parallel$ and $p_\perp$, we demand that $\mathrm{d}(\mathrm{Re}\,\Delta S) = 0$. With $E = (p_\parallel^2 + p_\perp^2)/2$ we have

$$\mathrm{d}\Delta S = (p_\parallel \mathrm{d}p_\parallel + p_\perp \mathrm{d}p_\perp)(t_2 - t_1) + (E + I_\mathrm{p})(\mathrm{d}t_2 - \mathrm{d}t_1) + \mathrm{d}p_\parallel \int_{t_1}^{t_2} \mathrm{d}\tau\, A(\tau)$$
$$+ p_\parallel\,[\mathrm{d}t_2 A(t_2) - \mathrm{d}t_1 A(t_1)] + \frac{1}{2}\left[\mathrm{d}t_2 A(t_2)^2 - \mathrm{d}t_1 A(t_1)^2\right]. \tag{13}$$

The coefficients of $\mathrm{d}t_1$ and $\mathrm{d}t_2$ are identically zero owing to the saddle-point equation (6). Hence we obtain the first-order nonlinear differential equation

$$\frac{\mathrm{d}E}{\mathrm{d}p_\parallel} = -\frac{1}{t_2 - t_1}\int_{t_1}^{t_2} \mathrm{d}\tau\, A(\tau), \tag{14}$$

where the right-hand sides depend on $p_\parallel$ and $p_\perp$ via t_2 and t_1. For the field (8),

$$\int_{t_1}^{t_2} \mathrm{d}\tau\, A(\tau) = \frac{A_0}{\omega}(\sin\omega t_2 - \sin\omega t_1) = \frac{2A_0}{\omega}\sin(\mathrm{Re}\,\omega t_2)\cosh(\mathrm{Im}\,\omega t_2), \tag{15}$$

where we used the properties (9) of the saddle-point solutions. Note that the differential equation (14) is actually real due to the reality of the integral (15).

For our field (8), the saddle-point times are given by ($p_\parallel > 0$)

$$\cos^2(\mathrm{Re}\,\omega t_2) = \frac{\alpha}{2} - \frac{1}{2}\sqrt{\alpha^2 - \frac{p_\parallel^2}{U_\mathrm{p}}}, \tag{16}$$

$$\cosh(\mathrm{Im}\,\omega t_2) = -\frac{p_\parallel}{2\sqrt{U_\mathrm{p}}\cos(\mathrm{Re}\,\omega t_2)}, \tag{17}$$

where

$$\alpha = 1 + \gamma^2 + \frac{E}{2U_\mathrm{p}} \tag{18}$$

and $\gamma = \sqrt{I_\mathrm{p}/(2U_\mathrm{p})}$ is the Keldysh parameter. In the limit where $p_\parallel \to 0$, we have $\cosh(\mathrm{Im}\,\omega t_2) \to \sqrt{\alpha}$. Given t_2, the other solution t_1 is specified by equation (9).

For $p_\parallel = 0$, we note that equation (16) implies that the two solutions t_2 and t_1 are half a period apart. Therefore, we have from equations (11) and (12) for $p_\parallel = 0$ that

$$\Delta S = \left(p_\perp^2/2 + I_\mathrm{p} + U_\mathrm{p}\right)\pi/\omega = m\pi. \tag{19}$$

For the ATI ring that corresponds to the absorption of N photons, c.f. equation (10), for $p_\parallel = 0$ we have

$$\tfrac{1}{2}p_\perp^2 + I_\mathrm{p} + U_\mathrm{p} = N\omega, \tag{20}$$

so that the destructive-interference condition reads

$$N = m. \tag{21}$$

Hence, for emission perpendicular to the laser polarization, on every other ATI ring (with net absorption of an odd (even) number of photons for even (odd) parity) we have a minimum.

Let us approximately solve the differential equation (14) with accuracy up to quadratic terms in $p_\parallel$ and $p_\perp$. For $p_\parallel^2 \ll U_\mathrm{p}$, the relevant quantities are ($p_\parallel > 0$)

$$\sin(\mathrm{Re}\,\omega t_2) = -1 + \frac{p_\parallel^2}{8U_\mathrm{p}\alpha}, \tag{22}$$

$$\cosh(\mathrm{Im}\,\omega t_2) = \sqrt{\alpha} - \frac{p_\parallel^2}{8U_\mathrm{p}\alpha^{3/2}}, \tag{23}$$

$$\omega(t_2 - t_1) = \pi - \frac{p_\parallel}{\sqrt{U_\mathrm{p}\alpha}} + O(p_\parallel^3). \tag{24}$$

With these approximations, the differential equation becomes ($p_\parallel > 0$)

$$p_\perp\frac{\mathrm{d}p_\perp}{\mathrm{d}p_\parallel} - \beta p_\perp^2 = \frac{2}{\pi^2\beta} - \left(1 - \frac{4}{\pi^2}\right)p_\parallel + \left(\frac{8}{\pi^2} - \frac{1}{1+\gamma^2}\right)\beta p_\parallel^2 + O(p_\parallel^3) \tag{25}$$

with

$$\beta = \frac{1}{2\pi\sqrt{U_\mathrm{p}(1+\gamma^2)}}. \tag{26}$$

We note that the left-hand side can be written as

$$\mathrm{e}^{2\beta p_\parallel}\frac{\mathrm{d}}{\mathrm{d}p_\parallel}\left(\frac{1}{2}p_\perp^2\mathrm{e}^{-2\beta p_\parallel}\right), \tag{27}$$

while the right-hand side depends only on $p_\parallel$. Hence, we can carry out the integration over $p_\parallel$. The constant of integration, which occurs in the process, is fixed so that for $p_\parallel = 0$ the curve starts on an ATI ring, which means that $p_\perp^2|_{p_\parallel=0}/2 = N\omega - I_\mathrm{p} - U_\mathrm{p}$. The resulting destructive-interference curve is an ellipse,

$$\frac{(p_\parallel - p)^2}{{a_\parallel}^2} + \frac{p_\perp^2}{a_\perp^2} = 1 \tag{28}$$

with

$$p = \frac{2\beta}{A}\left[N\omega - I_\mathrm{p} - U_\mathrm{p} + 4U_\mathrm{p}(1+\gamma^2)\right], \tag{29}$$

$$A = 1 - \frac{8}{\pi^2} - 4\beta^2(N\omega - I_\mathrm{p} - U_\mathrm{p}), \tag{30}$$

$$B = N\omega - I_\mathrm{p} - U_\mathrm{p} + \frac{A}{2}p^2 \tag{31}$$

and

$$a_\perp^2 = 2B, \quad a_\parallel^2 = 2B/A. \tag{32}$$

Where the curves intersect the $p_\perp$ axis, the slope is given by

$$p_\parallel = \frac{\sqrt{2(N\omega - I_\mathrm{p} - U_\mathrm{p})}}{2\beta\left[N\omega - I_\mathrm{p} - U_\mathrm{p} + 4U_\mathrm{p}(1+\gamma^2)\right]}\left[p_\perp - \sqrt{2(N\omega - I_\mathrm{p} - U_\mathrm{p})}\right]. \tag{33}$$

These approximate destructive-interference curves only make sense as long as $p < a_\parallel$, so that the curves intersect the $p_\perp$ axis. This is not the case for very large N when $A < 0$. Even before this limit is reached, the neglect of higher than quadratic terms may already become invalid. We will refer to the ellipses (28) as the set S1. Below, we will compare these curves with the full SFA.

There is a different class of solutions to equation (14), namely those that do not intersect the $p_\perp$ axis. Rather, they intersect the $p_\parallel$ axis at values $p_{\parallel n}$ with n given by equation (11). In the solution to equation (25) (or of equation (14) as long as $p_\parallel$ is no longer small), the constant of integration must be chosen accordingly. Note that the momenta $(0, p_{\parallel n})$ do not, in general, lie on ATI rings. Since obtaining an analogue of the solution (28) is cumbersome, we do not attempt it and will be satisfied with the numerical determination. We will refer to the set of these curves as S2.

The curves S1 and S2, along with the ATI rings, dominate the velocity maps for negative ions. As we will show below, they are differently affected by the Coulomb potential: the set S1 is distorted, but remains very prominent, especially near the $p_\perp$ axis. In contrast, the set S2 no longer plays a role in the Coulomb regime.

2.2. Zeros on an above-threshold ionization ring

A conspicuous feature is the number of interference nodes on a given ATI ring $E = \text{const}$. On top of any structure caused by $V(\mathbf{p}, t)$ (equation (4)), this is given by the difference of $\Delta S/(2\pi)$ at $\mathbf{p} = (p_\perp = 0,\ p_\parallel = \sqrt{2E})$ and at $\mathbf{p} = (p_\perp = \sqrt{2E},\ p_\parallel = 0)$:

$$\delta\Delta S \equiv \Delta S|_{p_\parallel=0}^{p_\parallel=\sqrt{2E}} = \int \mathrm{d}\Delta S. \tag{34}$$

From equations (13), (16) and (17), this is

$$\begin{aligned}\delta\Delta S &= \int_0^{\sqrt{2E}} \mathrm{d}p_\parallel \int_{t_1}^{t_2} \mathrm{d}\tau\, A(\tau) = \frac{2}{\omega}\int_0^{\sqrt{2E}} p_\parallel \mathrm{d}p_\parallel \tan(\mathrm{Re}\,\omega t_2) \\ &= \frac{2}{\omega}\int_0^{\sqrt{2E}} p_\parallel \mathrm{d}p_\parallel \sqrt{\frac{2-\alpha+\sqrt{\alpha^2 - p_\parallel^2/U_\mathrm{p}}}{\alpha-\sqrt{\alpha^2 - p_\parallel^2/U_\mathrm{p}}}},\end{aligned} \tag{35}$$

where $\alpha^2 - p_\parallel^2/U_\mathrm{p} > 0$. The integration is elementary and yields

$$\delta\Delta S = \frac{U_\mathrm{p}}{\omega}[(1+\beta_+)\sqrt{\beta_-(2-\beta_-)} + (2\alpha - 1)\arccos(1-\beta_-)] \tag{36}$$

with

$$\beta_\pm = \alpha \pm \sqrt{\alpha^2 - 2E/U_\mathrm{p}}. \tag{37}$$

If $M_\mathbf{p}$ is calculated to lowest-order perturbation theory so that absorption of exactly N photons is required to overcome the ionization potential, then the resulting angular distribution will be a superposition of spherical harmonics with angular momenta up to $\ell + N$, where ℓ denotes the angular momentum of the ground state. Chen *et al* [29] analysed the angular distribution for very low electron energy and found that in TDSE solutions the dominant angular momentum—the one that determines the observed angular pattern, i.e. the number of radial lobes in two-dimensional spectra—is roughly $N/2$ or slightly smaller, depending on the laser intensity. The SFA produces a smaller number of minima on an ATI ring with very low energy.

3. Numerical results

In order to illustrate the validity of the results obtained in the previous section and, for atoms, their limitation due to the effect of the Coulomb potential, in this section we present numerical results obtained by calculating the ionization (detachment) amplitude (1) (the direct SFA) and by solving the TDSE.

The direct ATD of negative ions can be described well using the SFA. The amplitude of direct ATD is obtained by calculating the integral over time t in equation (1). As examples, we will consider the negative hydrogen ion H^- and the negative fluorine ion F^-. The corresponding initial wave functions are modeled in accordance with [22] for H^- and with [30] for F^-. In the case of H^-, we model the initial wave functions by

$$\psi_\ell(\mathbf{r}) = (A/r)\exp(-\kappa r)Y_{\ell 0}(\hat{\mathbf{r}}), \tag{38}$$

with $\ell = 0$, $A = 0.75$, $\kappa = 0.235$ and $I_p = \kappa^2/2$. Similarly to [30, 31], we have checked that this ground state energy can be obtained using the potential

$$V(r) = -\left(\frac{1}{\sqrt{\alpha^2 + r^2}} + \frac{1}{\beta}\right) e^{-2r/\beta}, \tag{39}$$

with $\alpha = 0.5$ au and $\beta = 1.8469$ au. We used this potential to solve the TDSE for H^-. For the initial wave function of F^- we choose the Hartree–Fock-type wave function, which is given in analytical form as a series expansion in atomic Slater-type orbitals, while for the potential $V(r)$ we choose

$$V(r) = -a_1 \frac{e^{-\alpha_1 r}}{r} - a_2 \frac{e^{-\alpha_2 r}}{r}. \tag{40}$$

The parameters of the Slater-type orbitals and the potential $V(r)$ are given in [30]. The electron affinity of F^- is $I_p = 3.4$ eV. The potential (40) gives the correct ground-state energy, and its lowest p-orbital ($\ell = 1$) eigenfunction agrees well with our Hartree–Fock wave function. The effect of the Coulomb potential we will consider by solving the TDSE for the potential $V(r) = -1/r$ and comparing the obtained spectra with the SFA spectra for the 1s ground state.

We assume a linearly polarized laser field. For the TDSE calculation, we use the electric field vector with a cosine-square envelope and with a total pulse duration of n_p optical cycles, i.e. $T_p = n_p T$, $T = 2\pi/\omega$:

$$E(t) = E_0 \cos^2(\pi t/T_p) \cos \omega t \tag{41}$$

for $-T_p/2 \leqslant t \leqslant T_p/2$ and $E(t) = 0$ outside this interval. For the SFA calculations, we will use the pulse (41) or an infinitely long flat pulse.

The TDSE is solved using velocity gauge in dipole approximation as described in [30]. The algorithm used is a version of the method introduced in [32, 33]. The wave function is expanded in spherical harmonics and, after the operator splitting, the radial wave functions are propagated in time using the Crank–Nicolson approximation for the time-evolution operator. After propagation, angle-integrated and angle-resolved photoelectron spectra are obtained by analysing the final wave function using the fourth-order window-operator method [34].

3.1. Detachment velocity maps

In figure 2, the SFA velocity map for ATD of F^- is presented. The laser wavelength used (1800 nm) and the intensity (1.3×10^{13} W cm^{-2}) give $U_p/\omega = 5.71$, $N_{min} = 11$ and $\gamma = 0.6575$. Inspection of figure 2 shows that the SFA velocity map is dominated by the combined effect of the three sets of curves mentioned above: the ATD rings and the curves $\Delta S = m\pi$ that connect the interference minima and intersect the former. The set S1 of the $\Delta S = m\pi$ curves intersects the $p_\perp$ axis at the values $p_{\perp N} = \sqrt{2(N\omega - U_p - I_p)}$ on either the even-order (for odd ground-state parity) or the odd-order (for even ground-state parity) ATD rings. Since the parity of the F^- ground state is odd, these curves start at even-order ATD rings. In the first quadrant of figure 2 the curves S1 are represented by the white lines, which start at the ATD rings $N = 12$, 14, 16 and 18. It is obvious that these lines, given by the analytical results (28)–(32), are in excellent agreement with our numerical SFA results. The intersections of these curves with the ATD rings define a carpet-like pattern near perpendicular emission, which was experimentally observed in [35].

Finally, the curves of the second set (S2) do not intersect the $p_\perp$ axis. These curves can be obtained as solutions to the differential equation (14) with the initial condition that $\Delta S = m\pi$

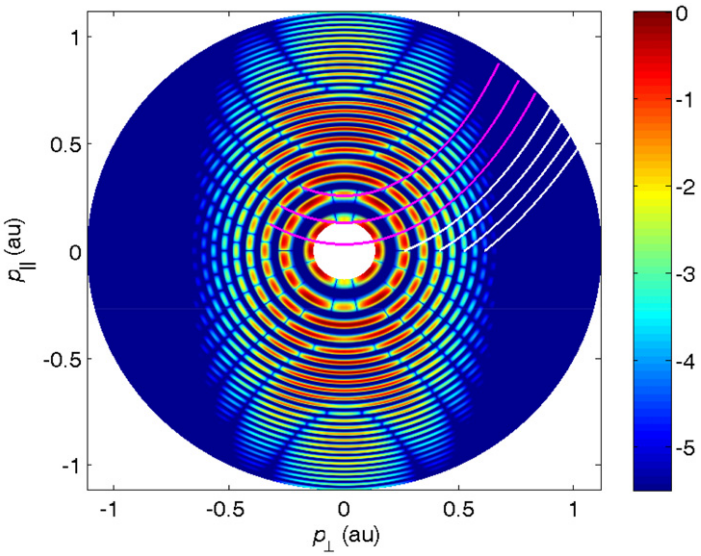

Figure 2. The logarithm of the differential detachment probability of F^-, presented in false colors, as a function of the detached electron momentum $\mathbf{p} = (p_\perp, p_\parallel)$ (in au). The wavelength and intensity of the linearly polarized laser field are 1800 nm and 1.3×10^{13} W cm^{-2}, respectively. The results are obtained using the direct SFA for an infinitely long flat pulse. The S1 curves (28) are entered as white lines in the first quadrant of the figure. Similarly, the S2 curves are entered as magenta lines.

at values $p_{\parallel m}$ and $p_\perp = 0$. They are presented by the magenta lines in figure 2. The velocity map shown in figure 2 very distinctly displays these curves. Off the $p_\parallel$ and $p_\perp$ axes, they are almost parallel to the curves S1. On the $p_\parallel$ axis, the set S2 specifies the destructive interference of the two intra-cycle quantum orbits, commonly known as the long and the short orbit, which are analogous to the 'ballistic interferences' in a constant force field; see, e.g., [36, 37]. The start times of these two orbits are closer together than half a period ($\omega(t_2 - t_1) < \pi$) so that the corresponding spacing in energy is larger than 2ω and increases with increasing $p_\parallel$ since $\omega(t_2 - t_1)$ is becoming smaller, as can be seen in figure 1.

According to equation (36), for the number of zeros on ATD rings in the first quadrant, viz $\delta\Delta S/(2\pi)$, we obtain: 1.54, 3.05, 4.07, 4.93, 5.69, 6.39, 7.05, 7.68 and 8.29 for the 1st, 2nd, 3rd, 4th, 5th, 6th, 7th, 8th and 9th rings ($N = 11, 12, \ldots, 19$), respectively. These numbers agree very well with the results presented in figure 2 (the corresponding numbers are 2, 3, 4, 5, 6, 6, 7, 8 and 9), which confirms the validity of the analytical result (36).

In figure 3 we present numerical results for a cosine-square pulse with a pulse duration of 18 cycles. It is obvious that the SFA and TDSE results agree very well. Also, in all cases the ATD rings and the structures S1 and S2 are well developed and confirm the results presented and commented on above. Comparison of the SFA and the TDSE velocity maps confirms that, in the momentum region covered by the figure, rescattering, which is not part of the SFA as formulated by equation (1), makes no significant contribution.

For H^- we first present the SFA results for an infinitely long flat pulse (figure 4) and then compare the SFA and TDSE results for a 6-cycle cosine-square pulse (figure 5). For the chosen

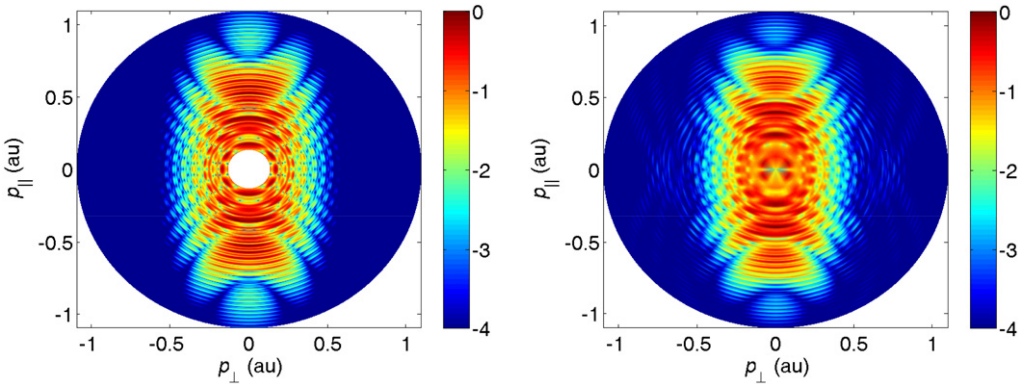

Figure 3. The same as in figure 2, but for a cosine-square pulse with total duration of 18 optical cycles. The results are obtained by using the direct SFA (left panel [38, 39]) and solving the TDSE (right panel).

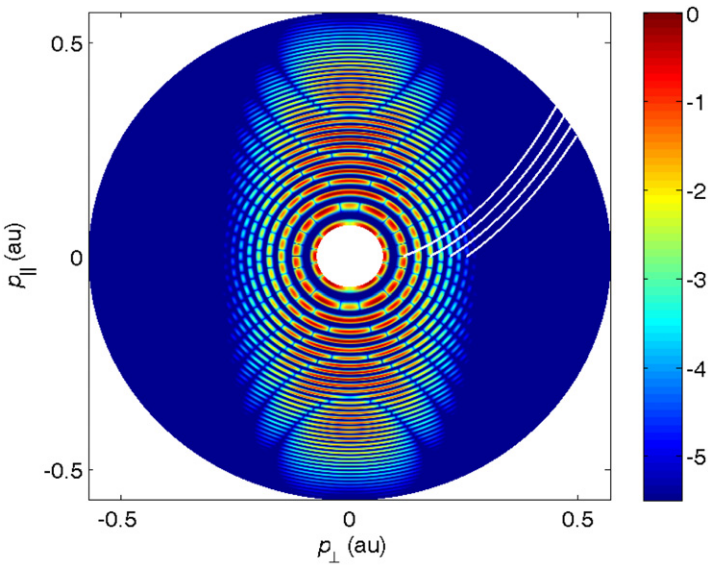

Figure 4. The logarithm of the differential detachment probability of H^-, presented in false colors, as a function of the detached electron momentum $\mathbf{p} = (p_\perp, p_\parallel)$ (in au). The wavelength and intensity of the linearly polarized laser field are 10 600 nm and 10^{11} W cm^{-2}, respectively. The results are obtained using the direct SFA for an infinitely long flat pulse. The curves (28) are entered as white lines in the first quadrant of the figure.

laser parameters we have $U_p/\omega = 8.97$, $N_{\min} = 16$ and $\gamma = 0.5984$. Since the ground state of H^- has even parity, the presented S1 curves start at the ATD rings that correspond to absorption of 17, 19, 21 and 23 photons. According to equation (36), for the number of zeros on the ATD rings in the first quadrant $\delta\Delta S/(2\pi)$, we obtain: 2.46, 4.04, 5.19, 6.16, 7.02, 7.81 and 8.55 for the 1st, 2nd, 3rd, 4th, 5th, 6th and 7th rings, respectively. These results again agree very well with the outcome of counting maxima on the ATI rings in figure 4.

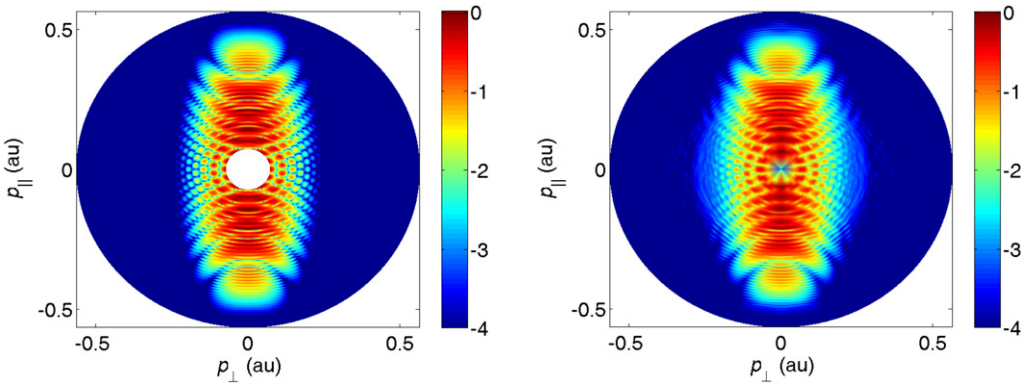

Figure 5. The same as in figure 4, but for a cosine-square pulse having total duration of six optical cycles. The results are obtained by using the direct SFA (left panel [38, 39]) and solving the TDSE (right panel).

Figure 5 demonstrates excellent agreement between the TDSE and the SFA results. The only difference that can be found is in the outer region where the yield is already very low. Here the TDSE does not resolve the interference structures quite as well as the SFA. It should be kept in mind that the TDSE, in contrast to the direct SFA, automatically includes rescattered electrons. For H^- and the current parameters, at the given accuracy there is no qualitative evidence of rescattering.

3.2. Ionization velocity maps for the hydrogen atom

In order to assess the consequences of the Coulomb potential, we turn to the hydrogen atom. In figure 6, we compare the velocity maps calculated from the TDSE (right-hand panels) with those from the SFA, where the Coulomb potential only enters via the ground-state wave function and, of course, the ionization potential. We present the results for three different intensities: 9×10^{13} W cm^{-2} ($U_p/\omega = 3.47$, $N_{min} = 13$ and $\gamma = 1.125$), 2.44×10^{14} W cm^{-2} ($U_p/\omega = 9.41$, $N_{min} = 19$ and $\gamma = 0.683$) and 4.55×10^{14} W cm^{-2} ($U_p/\omega = 17.5$, $N_{min} = 27$ and $\gamma = 0.5$).

As a general feature, we notice that the dependence on the transverse momentum is very different: the high-yield part of the TDSE spectra is narrower in the transverse direction, but rests on a more extended shelf, which is absent in the SFA, while it extends to quite high transverse momenta in the TDSE map. The former effect is clearly caused by Coulomb refocusing. The curves S1 and the carpet-like pattern around the transverse-momentum axis are present in both the SFA and the TDSE maps, but the curves as they turn away from the $p_\perp$ axis become steeper more quickly in the TDSE than in the SFA. The carpet-like pattern develops especially nicely in the TDSE for transverse momenta exceeding approximately 0.5 au.

In contrast, the curves S2 manifest themselves very differently in the SFA and the TDSE, that is, for negative ions and for atoms, so much so that one may ask if their underlying mechanism in the TDSE is still the same as in the SFA. In the SFA, the curves give the velocity map the appearance of a lobster tail with segments that are well separated all the way down to zero longitudinal momentum. In the TDSE, the map appears more like a candelabrum with arms that become almost parallel to the polarization axis for higher momenta. For higher intensities as shown in the middle and bottom panels of figure 6, the SFA and the TDSE maps become

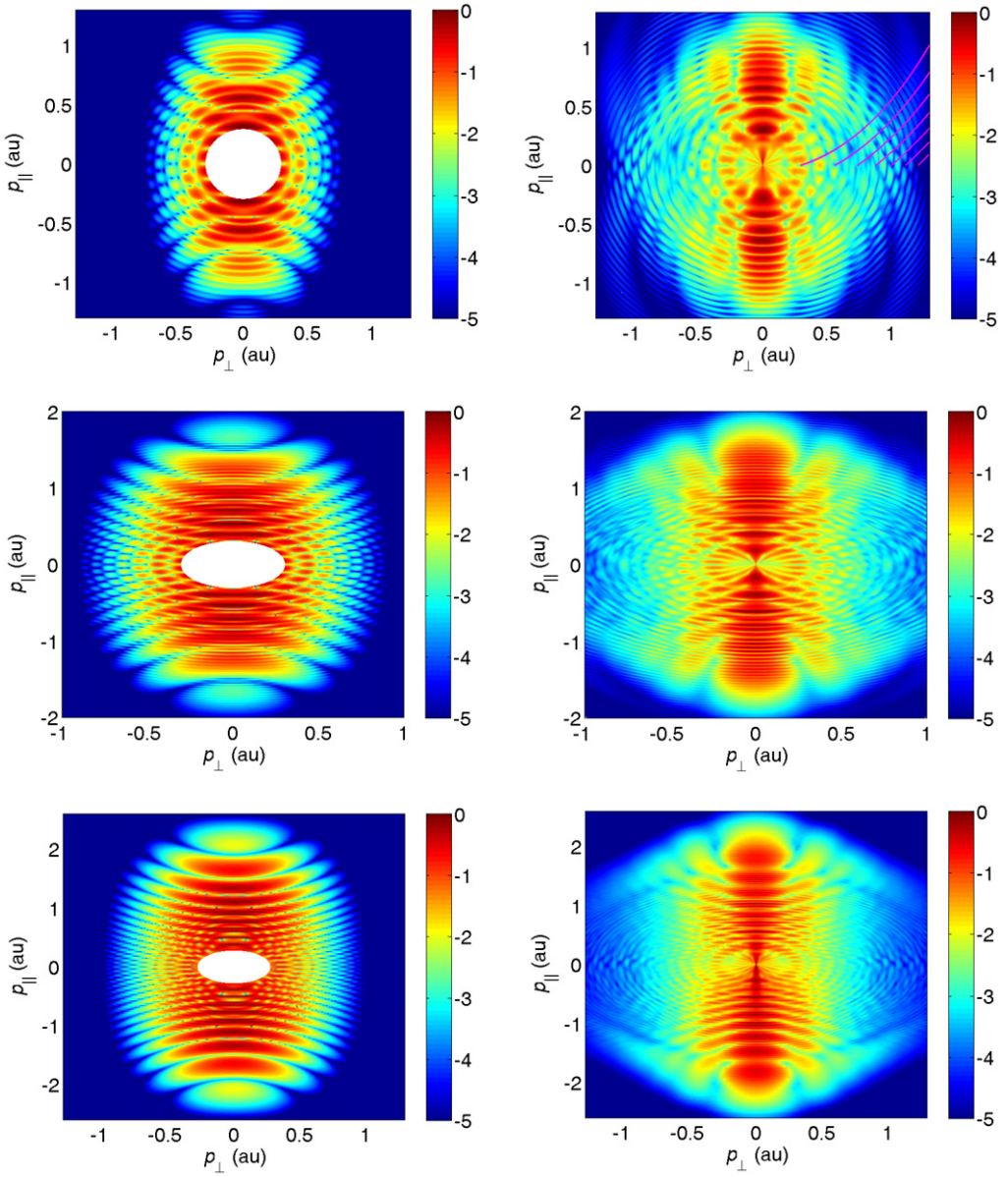

Figure 6. The logarithm of the differential ionization probability of H, presented in false colors, as a function of the ionized electron momentum $\mathbf{p} = (p_{\perp}, p_{\parallel})$ (in au). The wavelength of the linearly polarized laser field is 800 nm and the pulse shape is cosine square. The laser intensity and the total pulse duration, respectively, are 9×10^{13} W cm^{-2} and eight optical cycles (upper panels), 2.44×10^{14} W cm^{-2} and six cycles (middle panels) and 4.55×10^{14} W cm^{-2} and four cycles (bottom panels). The results are obtained using the direct SFA for few-cycle pulses (left panels) and solving the TDSE (right panels). Note that in the middle and lower panels the scales of the longitudinal and the perpendicular momentum are different. The red lines in the upper right panel represent the S1 curves (28).

more similar but remain qualitatively different, especially the S2 curves. Their manifestation in the TDSE is reminiscent of the patterns observed in [10, 40, 41], although in a very different parameter region, which were suggested to carry a hologram of the electron–ion interaction.

The fact that on the laser-polarization axis the minima due to the S2 interference are smoothed over by the action of a long-range potential is known [42]. On the other hand, for a negative ion, the structures caused by the S2 curves should become very prominent, unless they may be covered by rescattering contributions. A marked interference was observed for F^- in [43] at $p_\parallel = 0.69$ au. Figure 2, which is calculated at essentially the intensity of the experiment although not focally averaged, displays a destructive interference at $p_\parallel \approx 0.75$ au. Figure 2 exhibits three additional S2 minima on the $p_\parallel$ axis at lower momenta (on or near the ATI rings 11, 12 and 14), which cannot be identified in the data, since they only affect single ATI rings. The experimental angle-resolved energy spectra of [44] appear to reproduce the angle dependence of this S2 curve but a closer analysis is required.

3.3. Coulomb effects

In the SFA the influence of the atom on the ionization amplitude is only via the ground-state wave function. In the action (3), which mainly determines the shape of the spectrum, only the term $I_p t$ contains the ionization energy. The influence of the potential $V(\mathbf{r})$ can be taken into account in the semiclassical approximation in which the action takes the form

$$S^{(\mathrm{scl})}(\mathbf{p}, t) = \int^t \mathrm{d}\tau \left\{ V(\mathbf{r}_{\mathrm{cl}}(\tau)) + \frac{1}{2}\left[\mathbf{p} + \mathbf{A}(\tau) - \int^\tau \mathrm{d}t' \nabla V(\mathbf{r}_{\mathrm{cl}}(t'))\right]^2 \right\} + I_p t. \tag{42}$$

For the Coulomb potential we have

$$V(\mathbf{r}) = -1/r, \quad \nabla V(\mathbf{r}) = \mathbf{r}/r^3. \tag{43}$$

Comparing equations (3) and (42) we see that there are two main modifications of the action. The first contributes to the difference ΔS via $\int^t \mathrm{d}\tau [1/|\mathbf{r}_{\mathrm{cl}}^{(1)}(\tau)| - 1/|\mathbf{r}_{\mathrm{cl}}^{(2)}(\tau)|]$, where the upper index denotes orbits 1 and 2. The second modification is due to the change in the electron velocity by the term $\int^\tau \mathrm{d}t' \nabla V(\mathbf{r}_{\mathrm{cl}}(t'))$, which is also different for different orbits. It was argued that these two corrections have opposite signs so that the net effect is hard to assess [35]. The concept of quantum orbits can be maintained, but their calculation becomes considerably more complicated [24, 45]. The orbits that exist in the absence of the Coulomb field are modified and new orbits emerge that do not exist without the Coulomb field. The recalculation of the orbits is especially impeded by the fact that for a given final momentum the Coulomb-modified orbits depart from the ion at times different from those of the simple-man orbits.

The uppermost right panel of figure 6 again exhibits the S1 curves (28). These curves are depicted as red lines. It is clear that qualitatively they survive the Coulomb field, while quantitatively they are severely distorted. The number of minima evaluated from the SFA and the TDSE panels of figure 6 are roughly in agreement. On the lowest ATI ring, the SFA tends to underestimate the number of minima [29], while on the higher-energy rings the opposite tendency is found.

4. Conclusions

We investigated the interference structure imposed on ATD and ATI spectra by the contribution of the two distinct quantum orbits per field cycle that lead to the same final state. These orbits are

an element of theory, of the SFA, and the question that is most important for their interpretation is their physical reality. This can be answered by comparison of the spectra calculated via the SFA with those from the TDSE, which in this paper substitute the experiment. For ATD, in the absence of the long-range Coulomb potential, the agreement between the SFA and the TDSE is excellent. This underlines the fact that the quantum orbits and the simple-man picture closely capture the physical reality. All the destructive-interference curves predicted by the SFA and its quantum-orbit representation are quantitatively retrieved in the TDSE spectra. For ATI, the picture is more differentiated. We discriminated two types of destructive-interference curves: those that intersect the transverse and those that intersect the longitudinal momentum axis. The former remain clearly visible—in particular, the carpet-like pattern, which they produce in the velocity map for small longitudinal momenta, remains very distinct—while the latter all but disappear. We note that in some ways this carpet-like pattern can be thought of as an open-ended quantum carpet [46, 47] generated by two time windows without the presence of a bounding box.

Acknowledgments

We benefited from discussions with O Smirnova and W P Schleich. Sponsorship has been provided by the Alexander von Humboldt Foundation and funding by the German Federal Ministry of Education and Research in the framework of the Research Group Linkage Programme. This work was also funded by Deutsche Forschungsgemeinschaft (Sm-292/1 and Pa-730/4).

References

[1] Agostini P, Fabre F, Mainfray G, Petite G and Rahman N K 1979 *Phys. Rev. Lett.* **42** 112
[2] Keldysh L V 1964 *Zh. Eksp. Teor. Fiz.* **47** 1945
Keldysh L V 1965 *Sov. Phys.—JETP* **20** 1307 (Engl. transl.)
[3] Perelomov A M, Popov V S and Terent'ev M V 1966 *Zh. Eksp. Teor. Phys.* **50** 1393
Perelomov A M, Popov V S and Terent'ev M V 1966 *Sov. Phys.—JETP* **23** 924 (Engl. transl.)
[4] van Linden van den Heuvell H B and Muller H G 1998 *Multiphoton Processes (Cambridge Studies in Modern Optics* vol 8) ed S J Smith and P L Knight (Cambridge: Cambridge University Press) p 25
[5] Becker W, Grasbon F, Kopold R, Milošević D B, Paulus G G and Walther H 2002 *Adv. At. Mol. Opt. Phys.* **48** 35
[6] Agostini P and DiMauro L M 2008 *Contemp. Phys.* **49** 179
[7] Remetter T *et al* 2006 *Nature Phys.* **2** 323
[8] Gopal R *et al* 2009 *Phys. Rev. Lett.* **103** 053001
[9] Zherebtsov S *et al* 2011 *Nature Phys.* **7** 656
[10] Huismans Y *et al* 2011 *Science* **331** 61
[11] Lin C D, Le A-T, Chen Z, Morishita T and Lucchese R 2010 *J. Phys. B: At. Mol. Opt. Phys.* **43** 122001
[12] Faisal F H M 1973 *J. Phys. B: At. Mol. Phys.* **6** L89
[13] Reiss H R 1980 *Phys. Rev.* A **22** 1786
[14] Gribakin G F and Kuchiev M Yu 1997 *Phys. Rev.* A **55** 3760
[15] Goreslavskii S P, Popruzhenko S V, Shvetsov-Shilovskii N I and Shcherbachev O V 2005 *Zh. Eksp. Teor. Fiz.* **127** 27–36
Goreslavskii S P, Popruzhenko S V, Shvetsov-Shilovskii N I and Shcherbachev O V 2005 *Sov. Phys.—JETP* **100** 22–30 (Engl. transl.)

[16] Salières P *et al* 2001 *Science* **292** 902
[17] Kopold R, Becker W and Kleber M 2000 *Opt. Commun.* **179** 39
[18] Paulus G G, Grasbon F, Dreischuh A, Walther H, Kleber M and Becker W 2000 *Phys. Rev. Lett.* **84** 3791
[19] Milošević D B, Paulus G G and Becker W 2005 *Phys. Rev.* A **71** 061404
[20] Muller H G and Kooiman F C 1998 *Phys. Rev. Lett.* **81** 1207
[21] Arbó D G, Ishikawa K L, Schiessl K, Persson E and Burgdörfer J 2011 *Phys. Rev.* A **81** 021403
[22] Milošević D B, Gazibegović-Busuladžić A and Becker W 2003 *Phys. Rev.* A **68** 050702
Gazibegović-Busuladžić A, Milošević D B and Becker W 2004 *Phys. Rev.* A **70** 053403
[23] Blaga C I, Catoire F, Colosimo P, Paulus G G, Muller H G, Agostini P and DiMauro L F 2009 *Nature Phys.* **5** 335
Faisal F H M 2009 *Nature Phys.* **5** 319
[24] Yan T-M, Popruzhenko S V, Vrakking M J J and Bauer D 2010 *Phys. Rev. Lett.* **105** 253002
[25] Kästner A, Saalmann U and Rost J M 2012 *Phys. Rev. Lett.* **108** 033201
[26] Milošević D B and Becker W 2002 *Phys. Rev.* A **66** 063417
[27] Kopold R 2001 *Doctoral Dissertation* Technische Universität München
[28] Bauer D, Milošević D B and Becker W 2005 *Phys. Rev.* A **72** 023415
[29] Chen Z, Morishita T, Le A-T, Wickenhauser M, Tong X M and Lin C D 2006 *Phys. Rev.* A **74** 053405
[30] Fetić B, Milošević D B and Becker W 2011 *J. Mod. Opt.* **58** 1149–57
[31] Milošević D B, Čerkić A, Fetić B, Hasović E and Becker W 2010 *Laser Phys.* **20** 573–80
[32] Muller H G 1999 *Laser Phys.* **9** 138
Muller H G 1999 *Phys. Rev.* A **60** 1341
[33] Bauer D and Koval P 2006 *Comput. Phys. Commun.* **174** 396
[34] Schafer K J and Kulander K C 1990 *Phys. Rev.* A **42** 5794
Schafer K J 1991 *Comput. Phys. Commun.* **63** 427
[35] Korneev Ph A *et al* 2012 *Phys. Rev. Lett.* at press
[36] Bracher C, Becker W, Gurvitz S, Kleber M and Marinov M S 1998 *Am. J. Phys.* **66** 38
[37] Kramer T, Bracher C and Kleber M 2002 *J. Phys. A: Math. Gen.* **35** 8361
[38] Milošević D B, Paulus G G, Bauer D and Becker W 2006 *J. Phys. B: At. Mol. Opt. Phys.* **39** R203–62
[39] Milošević D B, Paulus G G and Becker W 2003 *Laser Phys.* **13** 948–58
[40] Bian X-B, Huismans Y, Smirnova O, Yuan K-J, Vrakking M J J and Bandrauk A D 2011 *Phys. Rev.* A **84** 043420
[41] Marchenko T, Huismans Y, Schafer K J and Vrakking M J J 2011 *Phys. Rev.* A **84** 053427
[42] Bauer D, Milošević D B and Becker W 2006 *J. Mod. Opt.* **53** 135
[43] Kiyan I Yu and Helm H P 2003 *Phys. Rev. Lett.* **90** 183001
[44] Gazibegović-Busuladžić A, Milošević D B, Becker W, Bergues B, Hultgren H and Kiyan I Yu 2010 *Phys. Rev. Lett.* **104** 103004
[45] Popruzhenko S V and Bauer D 2008 *J. Mod. Opt.* **55** 2573
Popruzhenko S V, Paulus G G and Bauer D 2008 *Phys. Rev.* A **77** 053409
[46] Marzoli I, Saif F, Bialynicki-Birula I, Friesch O M, Kaplan A E and Schleich W P 1998 *Acta Phys. Slovaca* **48** 323
[47] Kaplan A E, Marzoli I, Lamb W E Jr and Schleich W P 2000 *Phys. Rev.* A **61** 032101